Wheel Contact in Subway Collisions: Impact Testing of a Wheel-guard Countermeasure for Amputations, Transections and Decapitations

Daniel Hall, Jonathan Spears, Neal Morgan, Greg Shaw

Abstract Transportation injuries involving a pedestrian are often severely traumatic, particularly contact with subway trains. When trains impact pedestrians it frequently results in fatal injury, due to head, thoracic, and run-over injuries, and the number of fatalities is increasing. Yet, train safety research is under-represented in the literature when compared to automotive safety studies. The most common countermeasures proposed for subway systems focus on preventing pedestrian access to the rail path rather than reducing impact severity. Despite the obvious value of this approach in some environments, there is frequently insufficient space to retrofit these devices in a large portion of older subway stations. This work investigates the feasibility of a novel wheel-guard design to redirect pedestrians away from the path of the train wheels. The goal is to reduce near-certain fatality to moderate-to-severe injury risk. The design proposed accomplishes this survivability improvement in first contact with the wheels and head or limbs of a Hybrid-III anthropomorphic test device at velocities consistent with real-world train run-overs. As proposed, the design may not significantly reduce fatality risk when the torso is the point of contact, but improvements and development of similar designs are proposed by the authors.

Keywords Epidemiology, Impact Testing, Pedestrian Safety, Public Transportation, Safety Device Design.

I. INTRODUCTION

Subway-to-pedestrian collisions remain among the most severe trauma scenarios in transportation, often resulting in fatal injuries from head impacts, thoracic compression, or run-over events [1]. Automotive safety design has advanced significantly over the past century, with energy-absorbing front structures, standardised injury thresholds, and pedestrian crashworthiness testing. Unfortunately, similar protections are largely absent in the rail environment. The Metropolitan Transportation Authority (MTA) task force on subway trespassing reported a 20% rise in track intrusions between 2019 and 2021, and the number of pedestrian collisions has since risen above pre-pandemic levels: 241 incidents in 2024 compared to 185 in 2019 [2-4]. Despite this trend, the physical front-end design of subway trains has changed little with respect to pedestrian safety.

Safety design efforts in rail transit have primarily focused on collision avoidance, such as Platform Screen Doors (PSDs), which are barriers that align with train doors and open only when a train has come to a complete stop. PSDs have been implemented successfully in many global systems, including the newly constructed Victoria Line of the London Underground and the Shanghai Metro. Studies report that full-height PSDs can reduce suicide-related incidents by up to 90.9%, while three-quarter and half-height barriers reduce incidents by 79.2% and 60.2%, respectively [5-6]. While effective, PSDs face severe retrofitting constraints in older networks. An example is the New York City (NYC) Subway, where platform structure, train fleet diversity, and alignment tolerances limit feasibility to just 8.6% of stations under current conditions. Even under ideal alignment conditions, the percentage of feasible stations would rise to just 27%, underscoring the limitations of PSD-based solutions in NYC's context [7]. As a result, attention must shift toward passive safety strategies for systems that cannot accommodate PSDs, including train-mounted countermeasures that reduce injury severity when contact occurs.

While some focus has been given to front-end collision mitigation [8], one particularly hazardous injury mechanism is run-over contact with the leading wheels. Epidemiological reviews and baseline simulation studies have identified traumatic amputations and torso transections as frequent outcomes when pedestrians fall or lie in the track bed and are struck by the front of the train [9]. While some trains are equipped with rudimentary

D. Hall is a Postdoctoral Research Associate, J. Spears is a Research Assistant, N. Morgan is a Postdoctoral Research Associate, and G. Shaw is a Senior Scientist in the Center for Applied Biomechanics at the University of Virginia, Charlottesville, VA, USA. D. Hall is the corresponding author and can be contacted at hallda@virginia.edu

wheel guards designed to protect mechanical components from track debris, these offer little to no protection to pedestrians (Fig. 1). No publicly available data exist validating such structures for human safety.

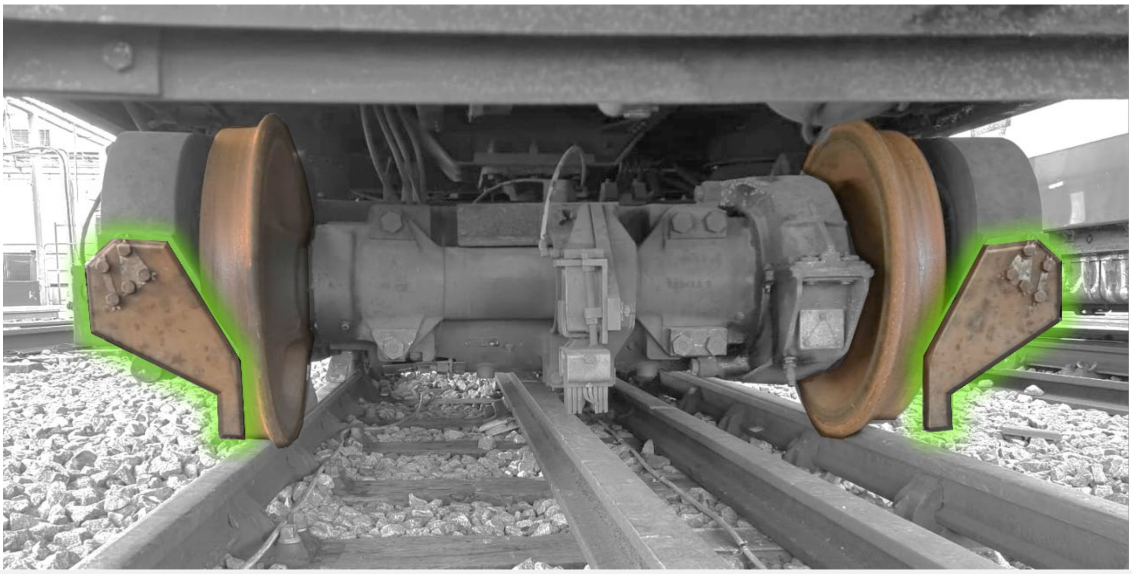

Fig. 1. **Train-mounted wheel guard (highlighted) used in London** U**nderground subway cars** (**image taken by author**).

This study addresses that gap by presenting a full-scale experimental evaluation of a novel energy-absorbing wheel guard designed to reduce injury severity during subway-to-pedestrian run-over collisions. The countermeasure consists of a deformable rubber structure mounted to the front of the train, shaped to redirect and cushion the limbs while limiting intrusion under the wheelset. To assess its safety performance, a series of impact tests was conducted using a Hybrid III anthropomorphic test device (ATD) across three target velocities: 6.7 m/s (15 mph), 8.9 m/s (20 mph), and 11.2 m/s (25 mph). The ATD was oriented in a range of postures to represent common real-world scenarios, including supine and partially upright positions.

The objectives of this paper are to:

1. Demonstrate the ability to limit intrusion of the pedestrian stand-in under the wheelset.
2. Evaluate the performance of a deformable train-mounted wheel guard in reducing head, chest, and limb injury severity in common subway impact scenarios.
3. Benchmark HIC15, DAMAGE, chest deflection, and limb deflections for a 50th male ATD collision with proposed wheel guard.
4. Determine whether the wheel guard offers a viable strategy for mitigating severe or fatal injury in pedestrian–subway collisions.

II. METHODS

Design of Countermeasure

A pair of wheel guards was fabricated for this investigation, one for each of the train’s leading wheels. The energy-absorbing element consisted of a sheet of neoprene rubber measuring 966 × 610 mm (38 c 24 inches), with a thickness of 25 mm (1 inch). The rubber was tightly clamped at both ends, forming an arch around a central steel plate 127 mm (5 inches) wide, see Fig. 2.

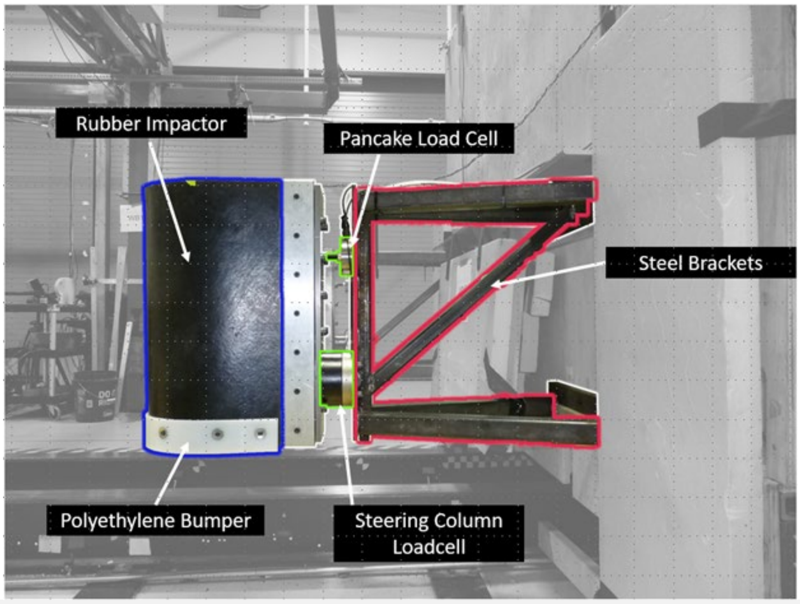

Fig. 2. **Fabricated wheel guard mounted to the test rig**.

To increase structural stiffness and prevent limb entrapment beneath the wheel guard, a polyethylene bumper measuring 75 mm × 838 mm × 6 mm was affixed along the outer edge of the rubber. Additionally, four 102 x 838 mm strips of rubber, each 13 mm thick, were secured to the interior underside. These features were refined through preliminary testing to strike a balance between rigidity and compliance, ensuring that limbs could not slip between wheel guard and "roadbed", while still allowing the structure to deform and absorb impact energy. In real-world service, the wheel guards would attach directly to the train's coupler limiters and ride along the rails and, unlike the laboratory set-up, no auxiliary brackets would be required. A SolidWorks model showing the intended integration with an R160 subway car is provided in Fig. 3. The concept design includes additional features, such as spring suspension and a vertical displacement limiter to allow closer clearance between wheel guard and rails; see Appendix for further details of proposed design.

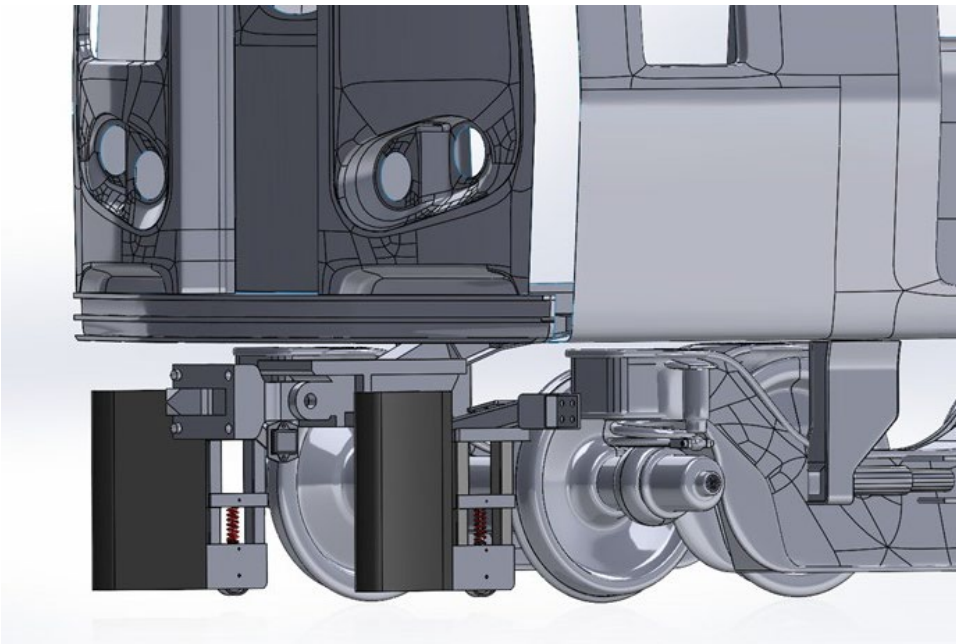

Fig. 3. **SolidWorks concept of the wheel guard integrated with the lead wheelset of a subway R160 train. In service, the guard would mount to the coupler limiters and ride directly on the rails.**

Experimental Testing

Test Facility and Set-up

The experimental testing was conducted at the Center for Applied Biomechanics (University of Virginia). Trains have much more mass and inertia than a pedestrian, allowing a train front to be replaced in testing by a stationary wall fixture. It is impractical to accelerate a train-equivalent mass in a laboratory environment, instead equivalent collision dynamics were obtained by propelling the posed ATD into the "train" front. The ATD was posed on a test fixture atop an acceleration sled and decoupled from the sled at the target velocity for each test.

The proxy train front consisted of a steel-reinforced plywood wall, designed to behave as a rigid structure. Two prototype wheel guards were mounted to this wall, positioned 10 mm (0.4 inches) above the rail surface and extending 1 m (39.4 inches) forward to replicate their intended placement ahead of the leading wheelset. In the lab, the guards were supported using custom-fabricated steel tubing brackets, suspending the guard 19 mm (0.75 inches) above rail height and constraining all motion except rubber compression.

Instrumentation

Instrumentation included:

- two six-axis load cells mounted at the expected head impact height;
- two single-axis Honeywell Model 41 pancake load cells, each placed atop a wheel guard.

These were installed between the neoprene rubber and the backing plate, transmitting load into welded steel brackets fixed to the wall. A trigger switch mounted along the track activated the off-board data acquisition system (DAS), synchronising:

- high-speed video;
- velocity gate measurements; and
- load cell data.

A photograph of the test rig and mounted wheel guard is shown in Fig. 2.

ATD and Positioning

The test subject was a Hybrid III 50th percentile male ATD, originally developed for frontal automotive crash testing. Because the instrumentation is designed for frontal impact loading, all tests were conducted with the ATD positioned laterally on its side, such that the front of the ATD made first contact with the wheel guard. This ensured the primary instrumentation zones aligned with the impact area. The ATD was aligned with rails spaced 1,420 mm (56 inches) apart, replicating New York City Subway track geometry. During sled acceleration, the ATD orientation was preserved using a retractable mechanical positioner, which was withdrawn just before impact to allow unrestrained motion into the guard.

Test Procedure

Each test followed the sequence of events illustrated in Fig. 4. The sled (light gray) was accelerated down the track (light blue) carrying the ATD (brown) restrained by the positioner (green). As the sled reached the target velocity, the positioner was withdrawn, allowing the ATD to continue forward unrestrained. The ATD then impacted the prototype wheel guard (black) at the prescribed velocity while the sled continued beneath the stage structure (light brown) and was pneumatically decelerated. Data collection concluded when any part of the ATD contacted the semi-rigid wall. See Appendix for additional time histories.

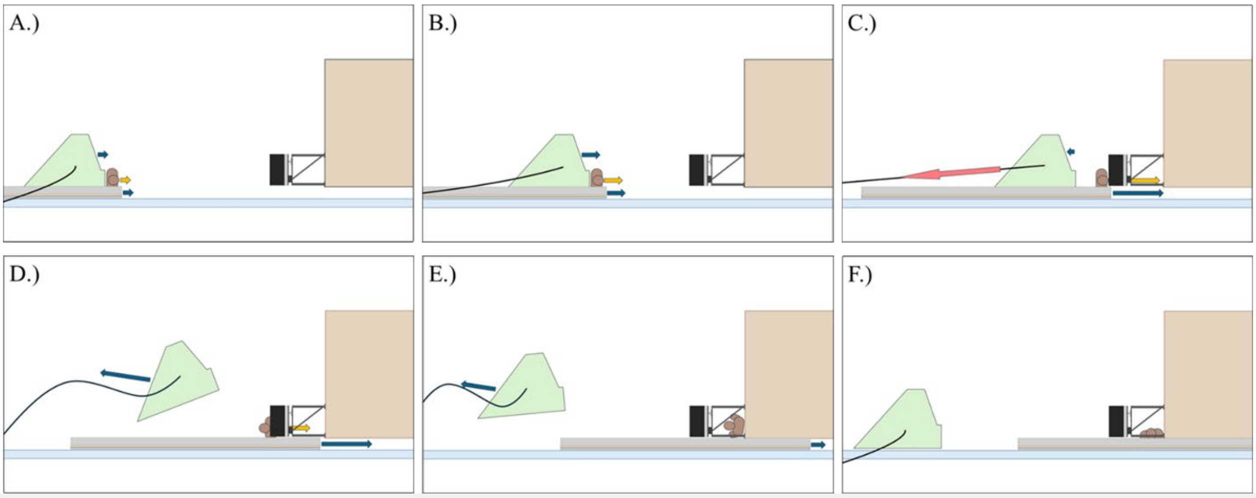

Fig. 4. Sequence of sled test events: (A) sled begins acceleration, (B) ATD and positioner accelerate with sled, (C) positioner is withdrawn just before impact, (D) ATD impacts the wheel guard, (E) ATD contacts semi-rigid wall as sled decelerates, (F) test concludes with sled and ATD at rest.

Test Matrix

Test conditions were selected based on trends identified in the previously discussed epidemiological analysis, which indicated frequent head, chest, and limb contacts at impact speeds between 6.7 m/s (15 mps) and 11.2 m/s (25 mph). Accordingly, tests were performed in three categories.

- **Head impacts**: ATD positioned for direct head contact with the guard at 6.7 m/s (15 mph), 8.9 m/s (20 mph), and 11.2 m/s (25 mph). Head resultant acceleration data were used to calculate HIC15 values and associated injury risk.
- **Chest impacts**: ATD positioned leaning over the rail for direct chest contact at 6.7 m/s and 8.9 m/s. Chest deflection (anterior to posterior, sternum to spine) was measured to estimate injury risk. The 11.2 m/s condition was omitted due to excessive ATD chest deflection at 8.9 m/s and risk of ATD damage.
- **Limb impacts**: ATD positioned with one or more limbs in the guard's path to assess whether the wheel guard redirected the limb away from the wheel trajectory. These outcomes were evaluated qualitatively based on ATD kinematics.

TABLE I
FULL TEST MATRIX

Test ID	Impact Region	Impact Velocity m/s (mph)	Injury Metric
H15	Head	6.7 (15)	HIC, Damage
H20	Head	8.9 (20)	HIC, Damage
H25	Head	11.2 (25)	HIC, Damage
T15	Thorax	6.7 (15)	Chest Deflection, Chest Acceleration
T20	Thorax	8.9 (20)	Chest Deflection, Chest Acceleration
UE25	Upper Extremities	11.2 (25)	Kinematics
LE25	Lower Extremities	11.2 (25)	Kinematics

Post-Processing and Data Analysis

Data collection began 50 ms prior to initial contact between the ATD and the wheel guard and continued until any part of the ATD impacted the rigid wall fixture, marking the end of meaningful kinematic and biomechanical response. All sensor data were collected via an off-board data-acquisition system and processed using custom Python scripts.

Signal Processing

All acceleration and force data were processed in accordance with SAE J211 filtering standards [10].

- Head and chest accelerations were filtered using a CFC 1000 channel class.

- Chest deflection signals were filtered at CFC 180.
- Load cell data (force) were processed with CFC 60.

Injury Metrics

Due to the high likelihood of complete traumatic amputation during wheel contact, limb injury risk was assessed qualitatively based on overall kinematics. A countermeasure was considered effective if the head or upper/lower extremity was redirected away from the wheel without snagging or being pulled beneath the guard and the chest deflection predicted a reasonable risk of injury.

Two head injury metrics were used to assess different mechanisms of injury. To estimate injury risk associated with skull fracture, the 15 ms Head Injury Criterion (HIC_{15}) was calculated from the filtered resultant head linear acceleration. The associated HIC_{15} Score was then converted to a probability of AIS4+ injury using the injury risk curve defined in [11]:

$$P_{HIC\ ,\ \ AIS4+} = \left[1 + e^{\left(4.9 + \frac{200}{HIC} - 0.00351 \times HIC\right)}\right]^{-1}$$

For rotational-based brain injury risk, the DAMAGE metric was calculated using filtered head angular accelerations. The corresponding probability of AIS4+ injury was computed using the following risk function developed in [12]:

$$P_{DAMAGE\ ,\ \ AIS4+} = 1 - e^{\left[-e^{\left(6.051 \times ln(0.957 \times DAMAGE + 0.017) - 6.051 \times ln(0.646)\right)}\right]}$$

Thoracic injury risk was assessed using chest deflection data recorded by the Hybrid III ATD's potentiometer, which is mounted at a single point on the sternum and measures anterior–posterior compression of the thorax. Specific injury risk curves exist to relate Hybrid III chest deflection to the probability of AIS3+ injury, with separate curves defined for various restraint conditions such as belt, airbag, or combined systems, as outlined in [13]. The choice of curve typically influences the resulting probability and depends heavily on the restraint mechanism involved. In this case, the wheel guard does not replicate any standard restraint condition. However, due to the high levels of chest deflection observed in these tests, the differences between the various risk curves are negligible. Therefore, the maximum chest deflection value (Dmax) was converted to a probability of AIS3+ injury using the general injury risk curves described in [14] :

$$P_{Dmax\ ,\ \ AIS3+} = 1 - e^{\left[-4.4444\left(\frac{Dmax}{e^{(4.5841 - (0.0214 * 45))}}\right)\right]}$$

III. RESULTS

Limb Contact (Amputations)

Figure 5 and Fig. 6 illustrate the kinematics of the Hybrid III upper and lower extremities during impact with the wheel guard at 11.2 m/s (25 mph), corresponding to tests UE25 and LE25, respectively. In both cases, the extremities make initial contact with the curved rubber surface of the wheel guard and are redirected laterally away from the wheel path. Notably, there were no observed instances of snagging, entrapment, or under-ride beneath the guard throughout the entire contact sequence.

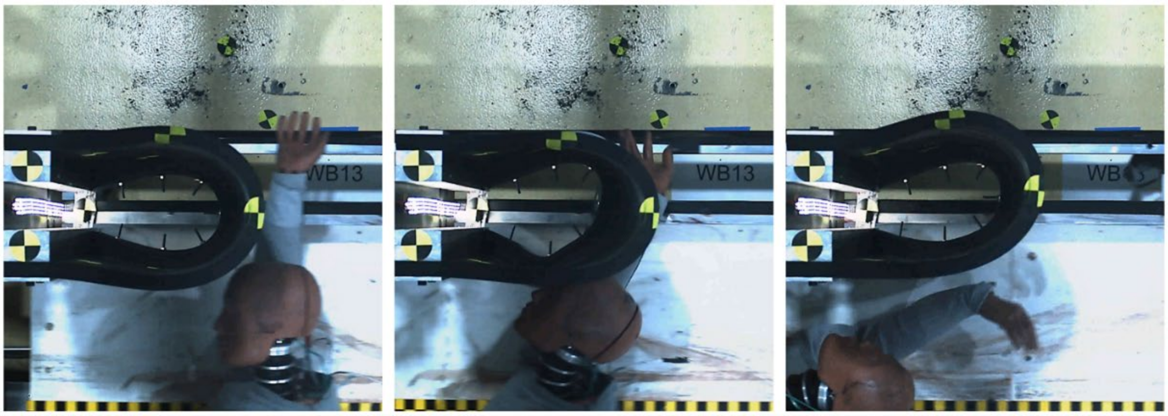

Fig. 5. **Upper-extremity kinematics during an 11 m/s (25 mph) impact**.

Fig. 6. **Lower-extremity kinematics during an 11 m/s (25 mph) impact**.

Thorax Impact

Both the 6.7 m/s (15 mph) and 8.9 m/s (20 mph) thorax impact tests resulted in chest deflections of 51 mm and 72 mm, respectively, corresponding to AIS3+ injury risks of 98% and 99%. Due to the high chest deflection observed at 8.9 m/s, an 11.2 m/s test was not performed to avoid damage to the Hybrid III chest potentiometer. Figure 7 shows the moment of peak chest deflection for each test.

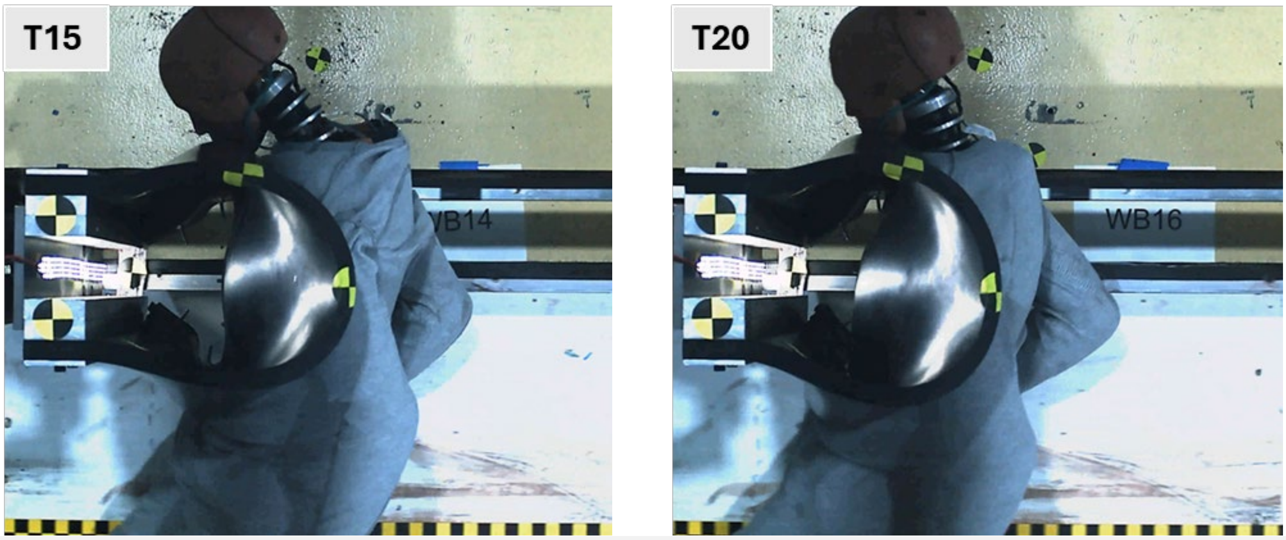

Fig. 7. **Chest maximum penetration for Tests T15 (*left*) and T20 (*right*)**.

Head Impact

The kinematics of the head during an 11.2 m/s (25 mph) direct impact with the wheel guard are shown in Fig. 8. The sequence begins at t = 0 ms (initial contact), with each subsequent frame captured at 10 ms intervals. In the early phase of the impact, the wheel guard deforms similarly to the chest impact tests. However, beginning around t = 20 ms, rotational head and neck motion becomes the dominant response. No visible bottoming-out of the wheel guard occurs, and the high-speed imagery suggests that a significant portion of the impact energy was redirected into rotational acceleration rather than linear deceleration.

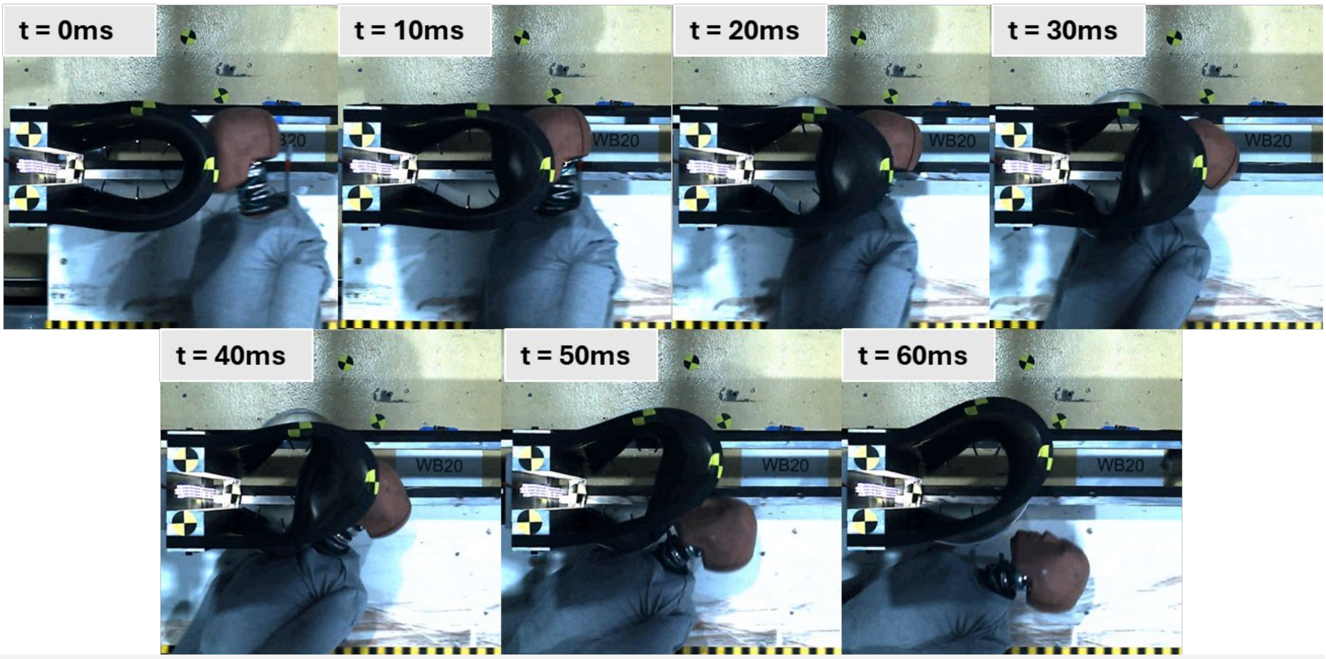

Fig. 8. **Head impact kinematics for Test H25**.

Figure 9. presents the AIS4+ injury risk associated with head impacts at three test velocities: 6.7 m/s (15 mph), 8.9 m/s (20 mph), and 11.2 m/s (25 mph). The test labelling is based on the velocity in mph. For each test, both the linear-based HIC_{15} metric and the rotational DAMAGE metric were used to estimate injury risk. The results show that while both risk values increase with velocity, the DAMAGE-based risk is consistently higher than the HIC-based risk at all test speeds. Horizontal dashed lines indicate the Euro NCAP 5-star (5%) and 3-star (35%) safety rating thresholds for head injury [15]. At 11.2 m/s, the DAMAGE metric exceeds the 3-star threshold, whereas the HIC-based risk remains below it, suggesting a higher sensitivity of rotational metrics to this impact configuration.

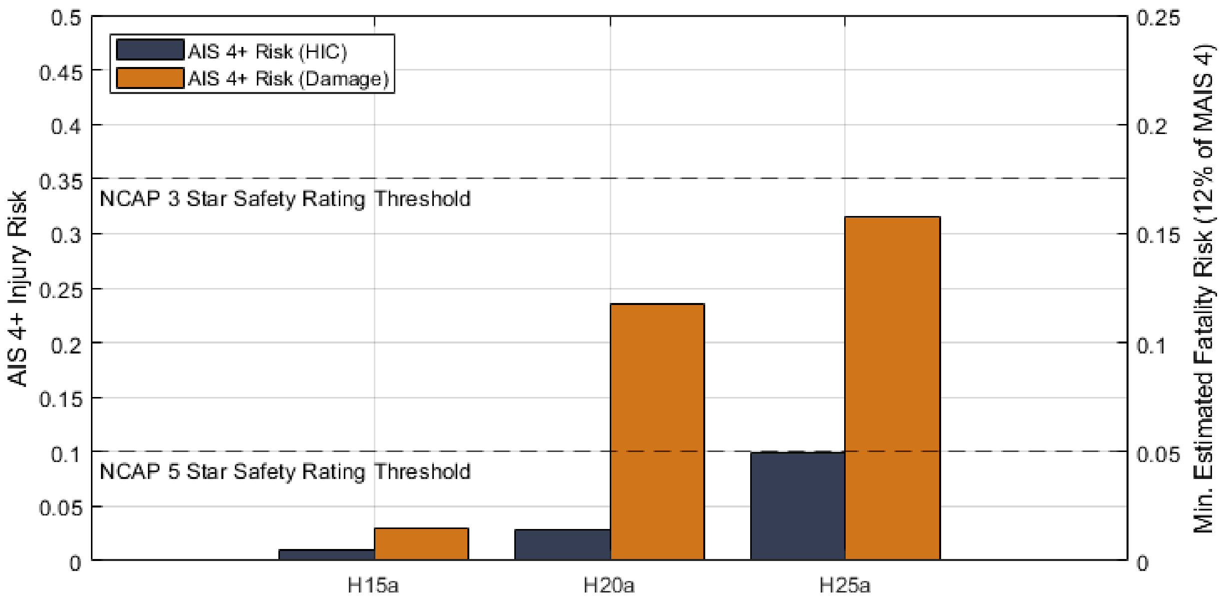

Fig. 9. **Head impacts: AIS4+ injury and estimated fatality risk**.

IV. DISCUSSION

This study evaluated a deformable train-mounted wheel guard designed to reduce injury severity in subway–pedestrian collisions. By simulating realistic impact conditions using a Hybrid III ATD and a range of velocities, the tests captured injury risk mechanisms across the limbs, chest, and head.

In the upper- and lower-extremity tests (UE25 and LE25), the impact velocity was held constant at 11.2 m/s (25 mph), as the primary objective was to evaluate limb kinematics rather than force-based injury metrics. The goal was to prevent complete traumatic amputations by redirecting limbs away from the path of the train's leading wheels. As illustrated in Figures 5 and 6, the deformable wheel guard effectively redirected both upper and lower limbs laterally, with no observed snagging, entrapment, or dragging. Although the Hybrid III ATD does not fully capture the anatomical variability present in human limbs, its geometry offers a first-pass approximation of the most affected demographic, i.e. adult males aged 35–40 years, who account for a majority of such incidents [4]. Future testing with alternative anthropometries, including paediatric and elderly surrogates, is warranted to assess population-wide effectiveness.

The thoracic impact tests (T15 and T20) produced high chest deflections of 51 mm and 72 mm at impact velocities of 6.7 m/s (15 mph) and 8.9 m/s (20 mph), translating to AIS3+ injury probabilities of 98% and 99%. These values reflect a high likelihood of serious thoracic trauma and highlight a limitation of the current wheel-guard configuration when the chest is the first point of contact. While these tests cannot directly quantify AIS4+ risk due to the absence of validated Hybrid III curves for that severity threshold, the near saturation of AIS3+ probability implies a strong likelihood of more severe outcomes.

Compared to the head and limbs, the thorax experienced the highest degree of penetration into the wheel guard, which is consistent with its greater mass and central location on the ATD. While the head and limbs were more easily redirected through rotation, the chest remained aligned with the impact direction for longer, resulting in deeper compression of the energy-absorbing material and correspondingly higher applied forces. Given that the wheel-guard response is force penetration dependent, this greater intrusion likely explains the elevated chest deflection and associated AIS3+ injury risk.

These findings suggest that additional energy absorption or geometric modifications, such as increased curvature or localised stiffness tuning, may be necessary to mitigate thoracic injury without compromising the redirection benefits seen in head and limb contacts. However, there is an important trade-off to consider. Epidemiological data indicate that direct chest-to-wheel impacts, including complete torso transections, are less common than limb-related run-over injuries [1]. Yet, while limb amputations can be survivable, severe thoracic injuries and decapitations are almost universally fatal. As such, even if these events occur less frequently, their lethality warrants serious consideration in countermeasure design. A balanced approach may involve tailoring the wheel guard's compliance profile to better accommodate high-mass impacts while preserving its redirection function for more frequent, survivable injuries.

The head impact tests provided the most comprehensive injury risk predictions among the three impact types, owing to the availability of both linear and rotational kinematic data across multiple velocities. As shown in Fig. 8, the impact sequence revealed an initial phase of wheel-guard deformation followed by a pronounced rotational response beginning around 20 ms. The redirection mechanism was consistent across all test speeds and successfully pushed the head laterally away from the wheel path without snagging, dragging, or bottoming-out of the guard. When redirection does not occur, the result may be skull fracture, basal trauma, or complete decapitation, the latter of which is almost universally fatal. The safety improvement observed in this study is therefore not a reduction from severe to moderate injury, but rather a shift from typically unsurvivable outcomes to potentially survivable ones. The ability of the wheel guard to absorb impact energy while redirecting the head away from the wheel path represents a meaningful step forward in mitigating high-severity injuries.

Figure 9 shows that rotational injury risk, as estimated by the DAMAGE metric, exceeded linear injury risk (HIC15) at all tested velocities. At 11.2 m/s (25 mph), the DAMAGE-predicted AIS4+ risk surpassed the Euro NCAP 3-star threshold of 35%, while the HIC-based risk remained below 10%. This discrepancy highlights the importance of incorporating rotational metrics into injury assessments, particularly for glancing or redirected impacts where linear acceleration alone may underestimate injury severity. While NCAP thresholds are useful for contextualising results, their original purpose must be considered. These thresholds were developed for automotive applications involving restrained occupants or low- to moderate-speed occupant impacts with smooth vehicle exteriors. In contrast, the present scenario involves a high-speed impact between a pedestrian and a train-mounted structure, making the injury environment significantly more severe than those addressed in standard NCAP testing.

The fact that rotational AIS4+ risk remains below 35%, and HIC-based risk remains well below critical thresholds, suggests a substantial reduction in expected injury severity. In other words, what would typically be considered a fatal head impact in a train collision has, through the inclusion of a deformable wheel guard, been reduced to an injury profile approaching that of a survivable automotive pedestrian impact.

There are limitations that must be noted. As previously discussed, some limitations to this work were related to the selection of the Hybrid III frontal impact ATD. The work herein is specific to a 50th male human surrogate striking a train face-on, and does not consider other directional loading scenarios. Human injury predictions can be very sensitive to directional loading of the head/neck and toros. Future studies with additional anthropometries, such as 95th percentile male, 05th percentile female, and child dummies, would confirm the viability of using wheel guards to reduce fatal wheel contacts to potentially survivable events for the entire population. Testing with additional instrumentation, side-impact dummies, or simulated human body models would allow for more accurate assessment of whole-body injury risks beyond those judged by this study to be the most immediately life-threatening.

The data gathered in this study are also limited to the first 50 ms of the initial impact event between the ATD and the train. We did not consider impacts that take longer than 50 ms, such as when the train is moving more slowly, or the subsequent impacts after initial wheel-guard contact. People have been injured when the train is moving at less than 4 m/s (9 mph) and when the train is stationary (falling onto the tracks). This suggests that train and track geometry can play a significant role in the pedestrian's injury outcomes and survival. The expanded range of physical and simulation testing proposed should also include additional environmental effects, such as components under the train carriage, rail-track crossmembers, and a more geometrically detailed train front, to better estimate the specific injury mechanisms involved in train-to-pedestrian impacts.

V. CONCLUSION

This study evaluated a deformable wheel guard designed to reduce the severity of injuries in subway–pedestrian collisions. Three impact regions (head, chest, and extremities) were tested across three velocities (6.7 m/s (15 mph), 8.9 m/s (20 mph), and 11.2 m/s (25 mph), based on recent epidemiological findings. Results demonstrated effective mitigation of limb injury risk through lateral redirection, as well as measurable reductions in head injury metrics. However, chest impacts at moderate speeds produced high probabilities of serious injuries, which highlights a potential trade-off in performance. The two head injury metrics used in this study highlight an important distinction. The wheel guard limited linear acceleration and successfully redirected the head away from the wheel path, but rotational forces remained high and became the dominant injury mechanism. In contrast, the chest experienced minimal redirection and deeper penetration into the guard, resulting in greater chest deflection. The combination of head and chest predicted injury outcomes emphasises a key challenge for future designs: balancing rotational and translational energy management across body regions to improve injury mitigation while maintaining system-wide effectiveness.

Despite the limitations mentioned above, the safety improvement observed in this study represents a shift from typically unsurvivable to more survivable outcomes. The ability of the wheel guard to absorb impact energy while redirecting the head away from the wheel path represents a meaningful step forward in mitigating high-severity injuries. The fact that rotational AIS4+ risk remains below 35%, and HIC-based risk remains well below critical thresholds, suggests a substantial reduction in expected injury severity. In other words, what would typically be considered a fatal head impact in a train collision has, through the inclusion of a deformable wheel guard, been reduced to an injury profile approaching that of a survivable automotive pedestrian impact. Further, run-over events are avoided for limb contact and potentially mitigated for glancing torso contacts. This represents a notable shift in approach: from exclusively focusing on collision prevention and avoidance to enabling a biomechanically manageable outcome in cases where contact cannot be avoided.

VI. ACKNOWLEDGEMENTS

This work was supported by the Federal Transit Administration (FTA). The authors gratefully acknowledge the support and collaboration of the Metropolitan Transportation Authority (MTA) in providing data, operational insight, and technical input throughout the project. The authors also thank the Center for Urban Transportation Research (CUTR) for their role as independent third-party evaluator, providing guidance and oversight to ensure the rigour and integrity of the research.

VII. REFERENCES

[1] Lin, P. T., Gill, J. R. (2009) Subway Train-Related Fatalities in New York City: Accident versus Suicide. *Journal of Forensic Sciences*, **54**: pp. 1414–1418.

[2] Martinez, J. (2024) As Subway Collisions Rise, Train Operators Feeling the Pain. *The City*.

[3] MTA Releases Track Trespassing Task Force Report. Available online: https://www.mta.info/press-release/mta-releases-track-trespassing-task-force-report (accessed 13 March 2026).

[4] Hall, D., Linogao, J., *et al*. (2023) Detailed Analysis of New York City Subway Pedestrian Incidents From 2019. *Transportation Research Record*, **2677**: pp. 642–650. doi:10.1177/03611981231166692.

[5] Chung, Y. W., Kang, S. J., Matsubayashi, T., Sawada, Y., Ueda, M. (2016) The Effectiveness of Platform Screen Doors for the Prevention of Subway Suicides in South Korea. *Journal of Affective Disorders*, **194**: pp. 80–83. doi:10.1016/j.jad.2016.01.026.

[6] Abdurrahman, U. T., Jack, A., Schmid, F. (2018) Effects of Platform Screen Doors on the Overall Railway System. *Proceedings of the 8th International Conference on Railway Engineering* IET, 2018, p. 6.

[7] STV Inc. (2020) New York City Transit SYSTEM-WIDE PLATFORM SCREEN DOOR FEASIBILITY STUDY 2020.

[8] Hall, D., Zentz, L., Lynch, P., Simms, C. (2025) Energy-Absorbing Countermeasures for Subway-to-Pedestrian Collisions: A Combined Experimental and Multibody Modelling Approach. *Applied Sciences*, **15**. doi:10.3390/app15116219.

[9] Hall, D., Gildea, K., Simms, C. (2024) Drainage Troughs as a Protective Measure in Subway–Pedestrian Collisions: A Multibody Model Evaluation. *Applied Sciences*, **14**. doi:10.3390/app142210738.

[10] Safety Test Instrumentation Standards Committee SAE International. *Instrumentation for Impact Test Part 1 - Electronic Instrumentation*. doi: 10.4271/J211/1_202208.

[11] Administration, N.H.T.S.; others FMVSS No. 201 (1995) Upper Interior Head Protection: Final Economic Assessment. US Department of Transportation, NHTSA, NTIS Office of Regulatory Analysis Plans and Policy, Washington D.C., USA.

[12] Gabler, L. F., Crandall, J. R., Panzer, M. B. (2019) Development of a Second-Order System for Rapid Estimation of Maximum Brain Strain. *Annals of Biomedical Engineering*, **47**: pp. 1971–1981. doi:10.1007/s10439-018-02179-9.

[13] Kent, R., Patrie, J., Benson, N. (2003) The Hybrid III Dummy as a Discriminator of Injurious and Non-Injurious Restraint Loading. *Annual Proceedings - Association for the Advancement of Automotive Medicine*, **47**: pp. 51–75.

[14] Poplin, G. S., McMurry, T.L., *et al*. (2017) Development of Thoracic Injury Risk Functions for the THOR ATD. *Accident Analysis & Prevention*, **106**: pp. 122–130. doi:10.1016/j.aap.2017.05.007.

[15] EURO NCAP ASSESSMENT PROTOCOL – VULNERABLE ROAD USER PROTECTION 2023.

VIII. APPENDIX

Appendix A: Test Designs

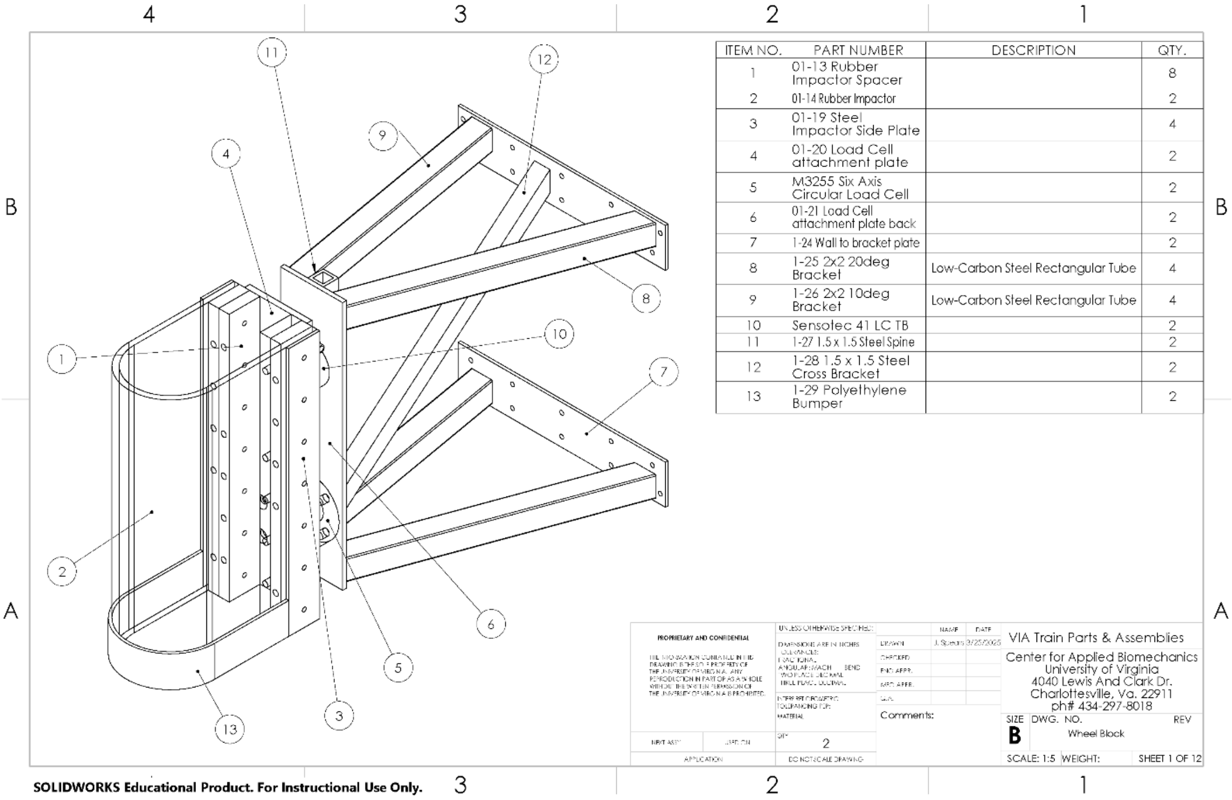

Fig. A1. Engineering drawing of wheel-guard testing device used in sled tests.

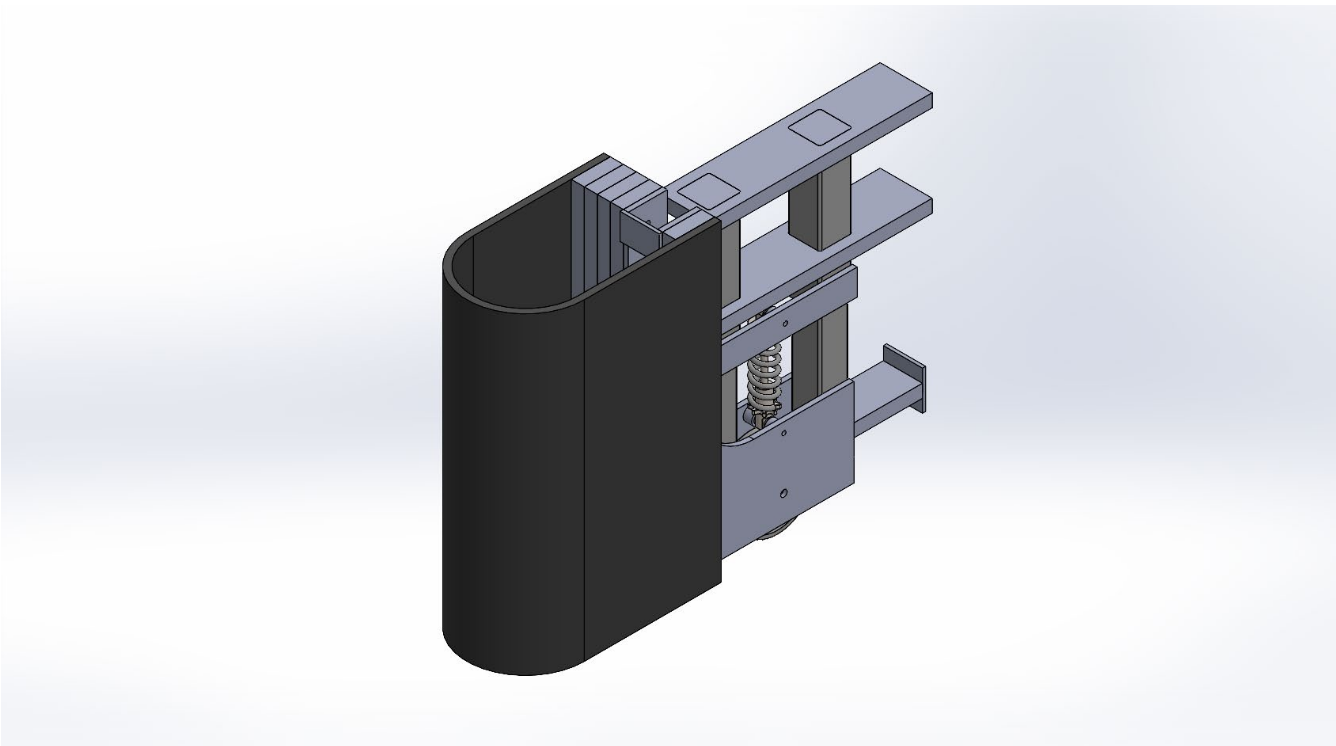

Fig. A2. Model of proposed wheel guard for R160 train wheels.

Appendix B: Test Timings and Metrics

Table BI outlines the important timings to consider when evaluating the Hybrid III time histories. As mentioned in the test procedure, the region of interest is between initial contact (set to time 0) and prior to contact with the semi-rigid wall.

TABLE BI

TEST IMPACT TIMINGS

Test ID	Impact Speed (mph)	Time Wheel Guard Contact Ends (s)	Time of Wall Contact (s)
UE25	25	0.026	0.013
T15	15.7	0.143	0.088
T20	20.7	0.122	0.059
H15	15.7	0.065	0.084
H20	20.7	0.059	0.064
LE25	25.7	0.318	0.053
H25	25.7	0.055	0.063

The calculated injury metrics for all tests are shown in Table BII.

TABLE BII

TEST IMPACT TIMINGS

Test ID	HIC15	HIC Time	HIC15: AIS2+ %	HIC15: AIS3+ %	Damage	Damage: AIS2+ %	Damage: AIS4+ %	Max. Chest Deflection (mm)	Chest AIS3+ %
UE25	93.6	0.122	6.56%	0.85%	0.546	84.58%	28.53%	19.6	0.04%
T15	294.5	0.221	0.20%	0.00%	0.365	34.21%	3.20%	51.2	8.62%
T20	172.7	0.162	1.70%	0.10%	0.427	52.45%	7.65%	72.5	77.98%
H15	175.6	0.174	2.28%	0.16%	0.36	32.79%	2.95%	10.6	0.01%
H20	194.6	0.13	9.82%	1.62%	0.525	80.21%	23.55%	9.1	0.01%
LE25	354.1	0.131	11.63%	2.14%	0.627	95.68%	53.02%	86.7	97.52%
H25	384.8	0.105	24.21%	7.20%	0.557	86.72%	31.54%	10.8	0.01%

Appendix C: Time History Plots

The section outlines the time histories for the head and chest impacts.

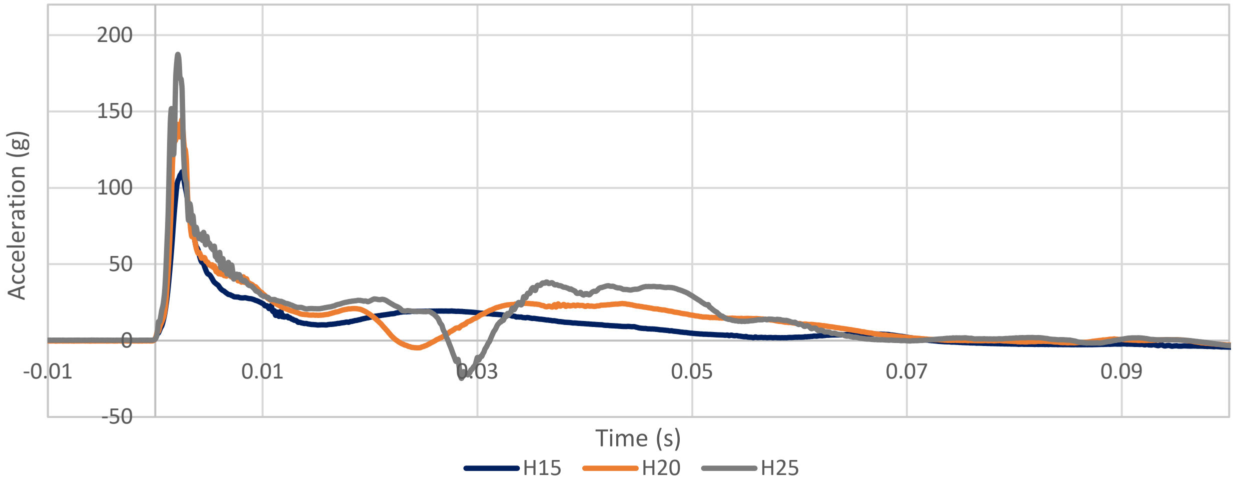

Fig. C1. Hybrid III Linear Head Acceleration – X direction.

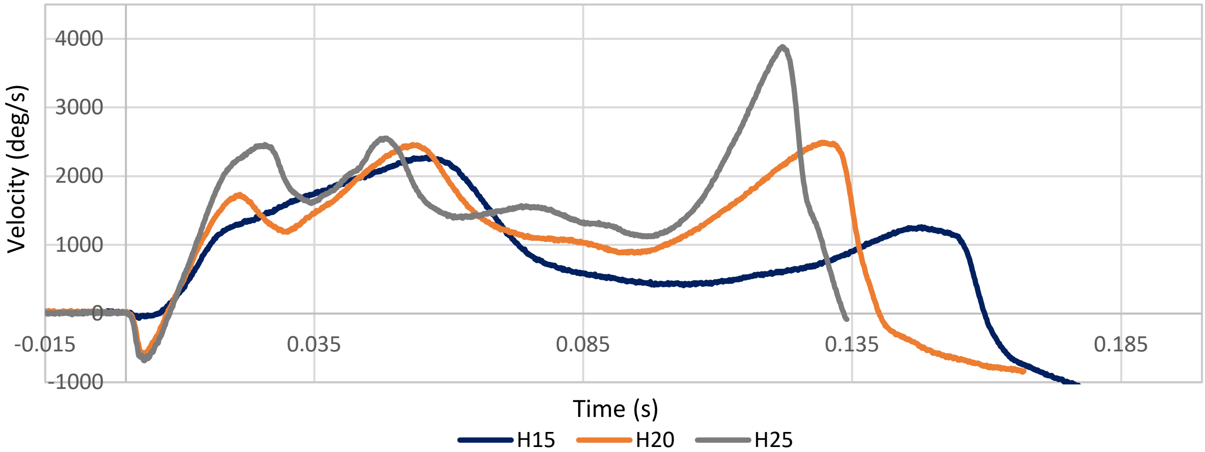

Fig. C2. Hybrid III Head Angular Velocity – Y axis.

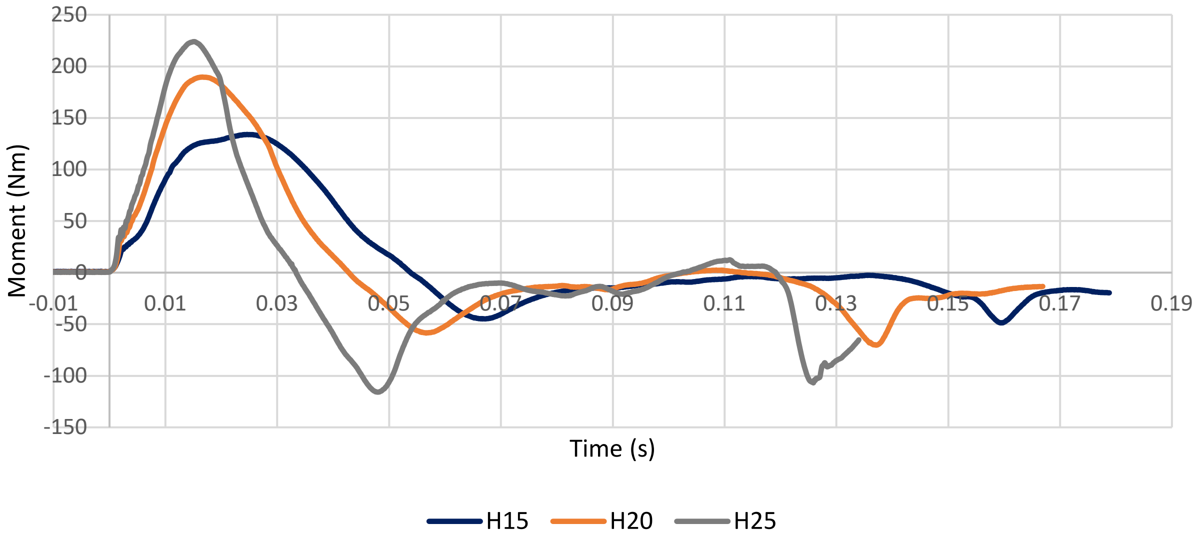

Fig. C3. Hybrid III Upper Neck Moments – Y axis.

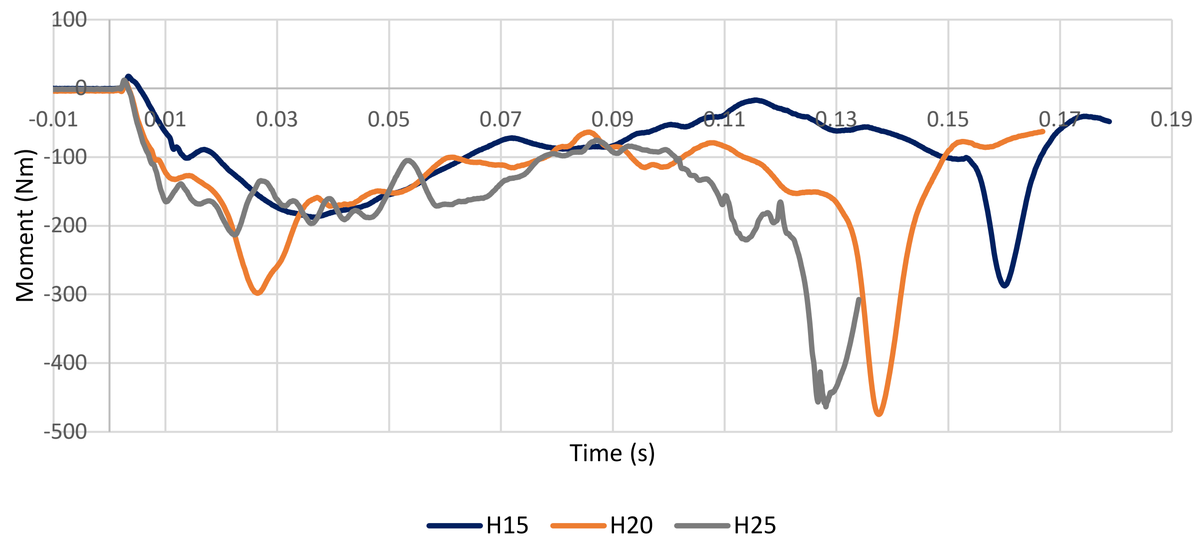

Fig. C4. Hybrid III Upper Neck Moments – Y axis.

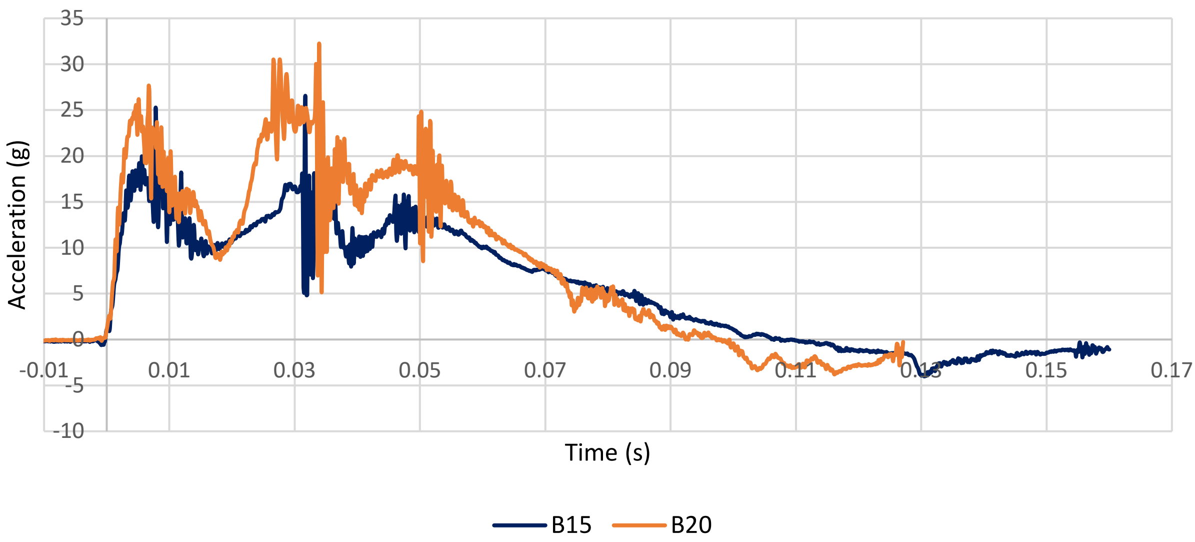

Fig. C5. Hybrid III Chest Acceleration – X axis.

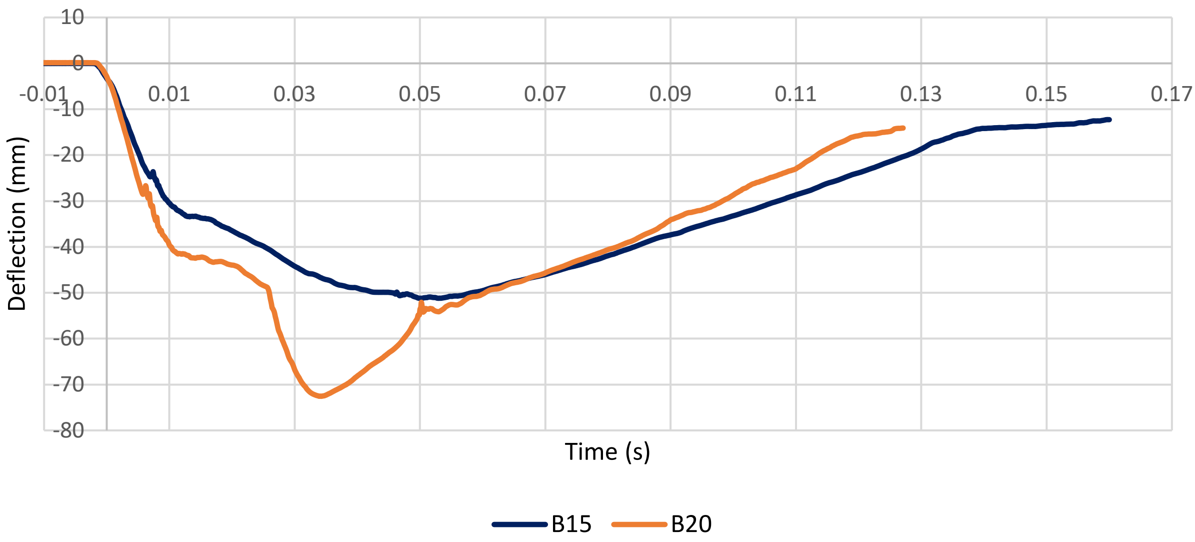

Fig. C6. Hybrid III Chest Deflection – X axis.

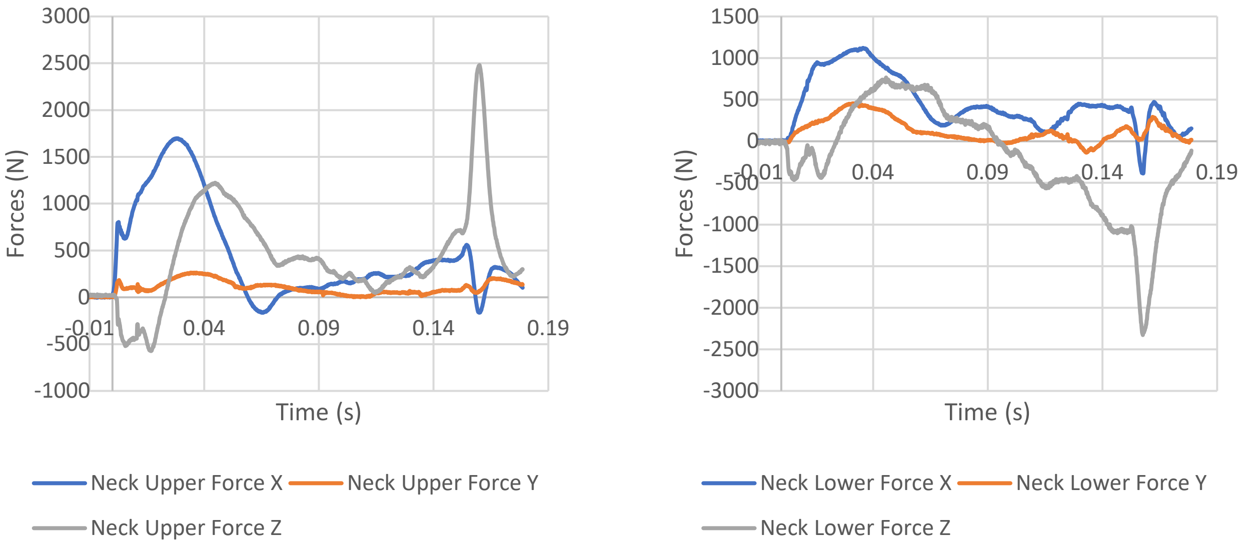

Fig. C7. Upper (***left***) and Lower (***right***) Neck Forces for Test H15.

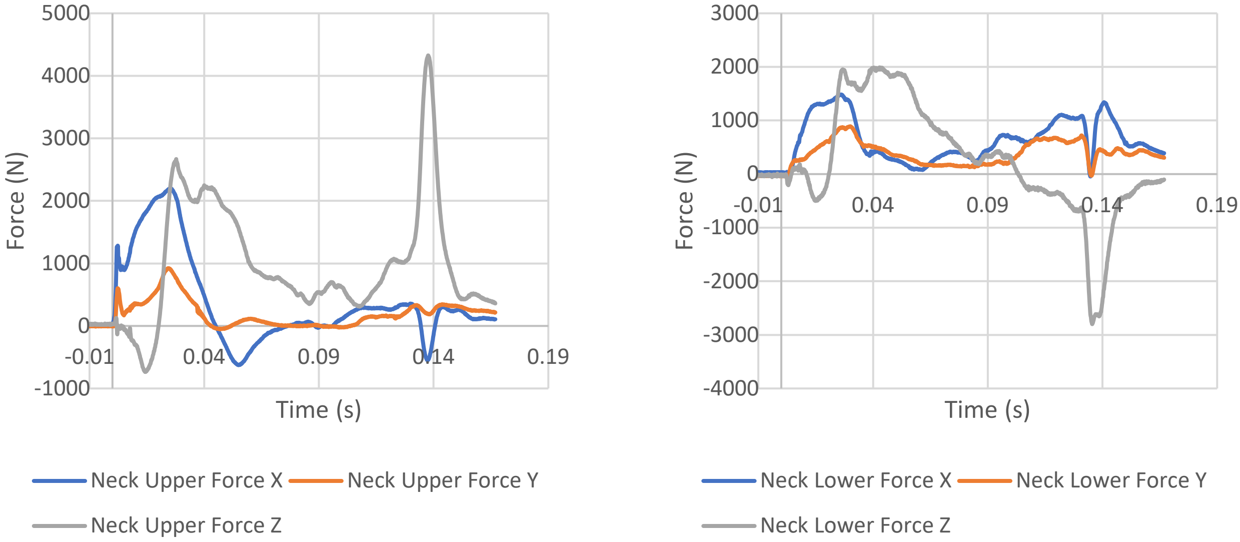

Fig. C8. Upper (***left***) and Lower (***right***) Neck Forces for Test H20.

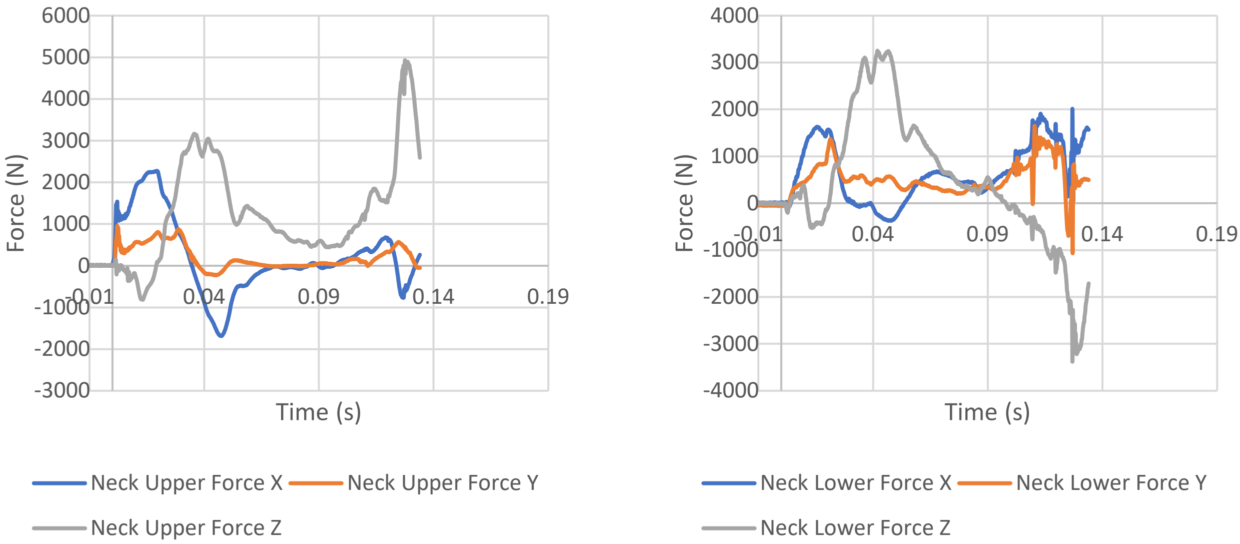

Fig. C9. Upper (***left***) and Lower (***right***) Neck Forces for Test H25.